Boehmite agglomeration through experimental and model approaches: From colloidal system to porous solid

Giulia Ferri, Severine Humbert, Mathieu Digne, Maxime Moreaud, Jean-Marc Schweitzer

▶ **To cite this version:**

Giulia Ferri, Severine Humbert, Mathieu Digne, Maxime Moreaud, Jean-Marc Schweitzer. Boehmite agglomeration through experimental and model approaches: From colloidal system to porous solid. Chemical Engineering Journal Advances, 2023, 14, pp.100497. 10.1016/j.ceja.2023.100497 . hal-04186758

HAL Id: hal-04186758
https://ifp.hal.science/hal-04186758

Submitted on 24 Aug 2023

HAL is a multi-disciplinary open access archive for the deposit and dissemination of scientific research documents, whether they are published or not. The documents may come from teaching and research institutions in France or abroad, or from public or private research centers.

L'archive ouverte pluridisciplinaire **HAL**, est destinée au dépôt et à la diffusion de documents scientifiques de niveau recherche, publiés ou non, émanant des établissements d'enseignement et de recherche français ou étrangers, des laboratoires publics ou privés.

Distributed under a Creative Commons Attribution - NonCommercial - NoDerivatives 4.0 International License

Chemical Engineering Journal Advances 14 (2023) 100497

Contents lists available at ScienceDirect

Chemical Engineering Journal Advances

journal homepage: www.sciencedirect.com/journal/chemical-engineering-journal-advances

Boehmite agglomeration through experimental and model approaches: From colloidal system to porous solid

Giulia Ferri [a,*], Severine Humbert [a], Mathieu Digne [a], Maxime Moreaud [a,b], Jean-Marc Schweitzer [a]

[a] IFP Energies nouvelles, Rond-point de l'changeur de Solaize, Solaize, 69360, France
[b] CMM MINES ParisTech, PSL-Research University, Fontainebleau, Seine-et-Marne, 77305, France

ARTICLE INFO

Keywords:
Colloidal agglomerates
Brownian dynamics
Population balance
Morphological model

ABSTRACT

The agglomeration dynamics within colloidal boehmite suspensions is crucial to understand the formation of a porous boehmite network during the manufacturing of γ-alumina catalyst carriers. Such carriers are frequently used in petroleum hydrotreating processes and must have specific textural characteristics. The method described in this work enables to model the three-dimensional morphology of colloidal agglomerates of boehmite for different conditions of pH in the colloidal mixture. These agglomerates are then used to generate a boehmite grain, whose textural properties can be numerically estimated. The coagulation kinetics has been studied with experimental Dynamic Light Scattering and Lagrangian model including Brownian dynamics and DLVO interaction potential. The adjustment of the Brownian aggregation kernel of a population-balance model enables to estimate the agglomerates size distribution and fractal dimension.

1. Introduction

Tuning the porosity of catalytic supports is attracting significant interest for the control of reaction kinetics in many industrial processes. γ-alumina catalytic supports, which cover the vast majority of the carriers used in the industry, are prepared from boehmite powder which undergoes several processing steps with different water content. Boehmite (the γ-alumina precursor) passes from the powder, to the paste and finally to the porous solid state. During these processes, structural changes occur at the meso- and macro-scale, which have an impact on the final porosity of the solid and on its performance as a catalytic support.

The structure of γ-alumina catalyst carrier is due to the organization of primary boehmite crystallites, of a few nm [1], formed during a precipitation phase. The primary crystallites assemble to form aggregates. The aggregates can coagulate to form larger aggregates and agglomerates. The shape of crystallites, aggregates and agglomerates determines the type of porosity at micro-, meso- and macro-scale [2].

In this work, agglomeration refers to the large-scale (from a few hundred nanometers to a few microns) assembly of aggregates by weak and reversible chemical interactions. While aggregation means the small-scale assembly of primary crystallites formed via strong, and irreversible bonds [3]. Since colloids of different scales (crystallites, aggregates, and agglomerates) are involved in the process, it is very challenging to obtain a complete understanding of the formation of boehmite morphology and of its fractal structure. The growth of aggregates and agglomerates takes place when particles meet in the reaction environment and are a consequence of different interactions.

Light-scattering techniques are widely used for the study of colloidal assembling and enable to estimate the fractal dimension of boehmite suspensions [4,5]. These studies focus on the aggregation of elementary crystallites. But there is currently a limited understanding of agglomeration and of the boehmite assembling process on multiple-scales.

Regarding the modeling of colloidal assembly, for small-scales Lagrangian models (like Brownian Dynamics) [6] simulate fast coagulation kinetics, which cannot be measured experimentally, and provide morphological properties of the formed structures. These methods enable to simulate, however, a limited number of colloidal particles, due to high computational time. To extend the particles number up to 10^{21}, the population-balance equation is often used [7]. This approach is based on the expressions of assembling and breakage kernels which can be either analytical [8] or empirical [9]. The novelty proposed by this work is to use both models to investigate the phenomenon of colloidal boehmite agglomeration. The results make it possible to build the

* Corresponding author at: Politecnico di Milano, Dipartimento di Energia, Via La Masa 34, Milano, 20156, Italy
E-mail address: giulia.ferri@polimi.it (G. Ferri).

https://doi.org/10.1016/j.ceja.2023.100497

Available online 14 April 2023
2666-8211/© 2023 The Authors. Published by Elsevier B.V. This is an open access article under the CC BY-NC-ND license (http://creativecommons.org/licenses/by-nc-nd/4.0/).

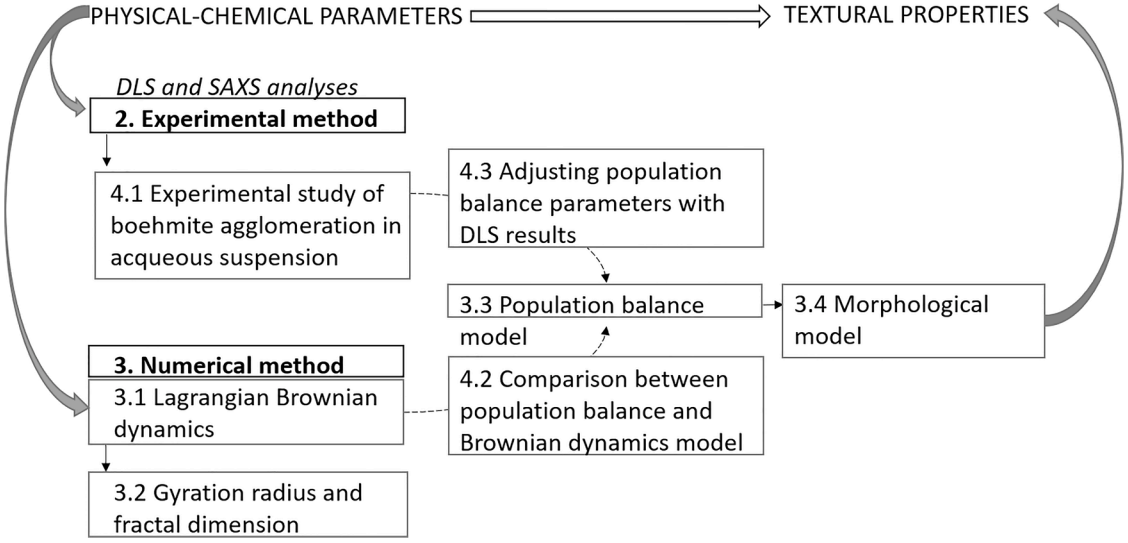

Fig. 1. Strategy to estimate textural properties of a boehmite porous solid according to the physical-chemical parameters of Brownian agglomeration.

morphological model of the agglomeration network.

Our strategy (see Fig. 1) enables to describe the morphology of the solid structure as a result of the chemical composition of a colloidal suspension. To this purpose, ideal and low concentration boehmite suspensions have been studied under Brownian conditions. These systems have been described using theoretical models of colloidal agglomeration (like DLVO theory [10,11] and Smoluchowski equation [8]). The boehmite colloidal suspensions are experimentally characterised during coagulation via DLS (dynamic light scattering), in order to provide data for the adjustment of the aggregation kernels of a population-balance model.

A discrete-element model, relying on DLVO and Langevin [12] theories, enables to fill the experimental gaps and to estimate the evolution of average radius and fractal dimension along the agglomeration process. The fractal dimension d_f is here considered as a structural parameter to characterize individual agglomerates.

The Lagrangian approach and the population balance can represent agglomeration under Brownian motion and a validation is possible between these two modeling approaches. These models both depend on the Fuchs stability coefficient, which is a function of the pH and ionic strength of the colloidal suspension. The Fuchs stability ratio W reaches a value close to unity for strongly unstable suspensions which have a high tendency to agglomerate [13], its theoretical value can be computed from the DLVO interaction potential U^{tot}

$$W \approx \frac{1}{2\,\kappa\,a}\exp\left(\frac{U^{tot,max}}{k_B T}\right) \tag{1}$$

assuming spherical particles of radius a, homogeneous surface charge distribution and negligible solvation force. r is the distance between the centers of the two particles, k_B is the Boltzmann constant and T is the temperature.

$$\kappa = \left(\frac{\varepsilon\, k_B\, T}{2\, e^2\, A_v}\right)^{-0.5}\sqrt{I} \tag{2}$$

is the inverse of the Debye length, the length of the layer of ions that are strongly bond to the particles and screen the electrical field of the particle. In the Eq.(2) ε is the electric permittivity, e is the electron charge, $A_v$is the Avogadro number and I is the ionic strength of the colloidal suspension. The Lagrangian model input parameters are the size of the primary particles, the boehmite concentration and W. The model result is a dependence of the fractal dimension on the gyration radius. This dependence justifies the consideration of a size-dependent fractal dimension and is an input of the population balance, where the Smoluchowski kernel is considered. The population balance also depends on the size distribution of the primary dispersed boehmite particles (in our case a Dirac function), on W and on the boehmite concentration. The result of the population balance is the size distribution of the boehmite agglomerates at the end of the agglomeration process.

The relationship between the fractal dimension and the agglomerate gyration radius, and the agglomerate size distribution are the input parameters of a morphological agglomeration model [14], whose result is the final morphology of an agglomerates assembly. This last model is based on a random sequential addition algorithm and on morphological operators. It does not describe the coagulation physics but simulates a stochastic assembly of particles. Such a model is suitable for the simulation of a realistically large morphology, which makes possible the estimation of textural properties.

2. Experimental methods

Boehmite suspensions were prepared using a highly dispersible powder (Pural SB3, from Sasol GmbH) with a loss on ignition of 26%. The suspension was prepared with a concentration of boehmite powder of 0.04 g/L. The boehmite concentration was chosen according to the measurement techniques. Indeed, the coagulation time scale must be of the same order of magnitude of the acquisition time. The nitric acid (1 M Fisher Scientific J/5550/PB15) concentration has been chosen to peptize the boehmite powder at a pH around 3, 0.0015 M To control the pH, ammonia has been injected (1 M Chem-Lab CL05.0101.1000). The pH was measured using a pH-meter (Seven2Go Mettler Toledo).

The zeta potential measurements were performed with Malvern Zetasizer Nano ZS with 1 mL sample using capillary cells with electrodes.

A study of the titration curve and the corresponding zeta potential vs pH curves was realized to tune the zeta potential via NH_3 injection in the initial peptized boehmite suspension.

DLS measurement were performed with Malvern Zetasizer Nano ZS, using square polysyrene cell, which have been filled with 1 mL of initial peptized suspension. Filtering the suspension with a syringe filter at 5 µm was necessary to remove any dust that could falsify the measurement and to eliminate the few grains of un-peptized powder that would not be visible with DLS. After the characterization of the initial suspension, 0.2 ml of ammonia solution was injected in the measurement cell and the in-situ analysis was started. The average diameter was computed with the cumulant method [15].

SAXS analyses were performed at the SWING beamline of SOLEIL synchrotron in Saint Aubin, France. The incident energy of the X-ray beam was 10 keV. 200 mL of the initial suspension were placed in a stirred reactor, the sample was pumped continuously through a quartz capillary of 1.5 mm. The injection of 40 ml of the ammonia was achieved via remote control of two syringes. The average gyration radius and fractal dimension was computed using the Beaucage model [16].

STEM images have been acquired using a FEI Nova NanoSEM microscope operating at 15 keV. The microscope is equipped with a STEM detector. A droplet of 10 µL of the sample is deposited on copper grids and dried under IR lamp. The carbon membrane covering the grid has no holes.

3. Numerical methods

Three numerical approaches were used to model the colloidal agglomeration process and the morphology of the agglomerates. Concerning the agglomeration process, the two models were Brownian dynamics and population balance equation. The first enabled to simulate fast agglomeration kinetics, which cannot be observed experimentally, giving insight into the evolution of the size and fractal dimension of agglomerates in a system under Brownian conditions with a DLVO interaction potential. The drawback was, however, the computation time, which was very high for the simulation of large systems. The second, the population balance, enabled to simulate the evolution of a system consisting of a large number of particles.

A third model, based on the stochastic packings of elementary objects, was used to build the morphology of colloidal agglomerates.

3.1. Lagrangian Brownian dynamics

The Lagrangian model was described in a previous work [14]. The particle radius of 40 nm agrees with the size of the primary boehmite aggregates measured with DLS analysis. The particle number is 2048, which is the result of considering 1% volume concentration of solid particles in a cube of 3800 nm side length. These conditions enable the simulation of an agglomeration time of 0.27 s in 27 computing days (2.60 GHz CPU), which we consider reasonable for our study. A random sequential addition algorithm was used to generate the initial positions of the spheres. The dynamics of each sphere i was computed via the momentum balance

$$m_i \cdot \overrightarrow{a_i} = \sum_{i \neq j} \overrightarrow{F_{ij}} + \overrightarrow{F_i^R} + \overrightarrow{F_i^D}, \tag{3}$$

where m_i and a_i are the mass and the acceleration of the particle. $\overrightarrow{F_{ij}}$ is the DLVO interaction force deriving from DLVO potential [10]. The model accounts for the interaction between the particle i and all the other particles i contained within an interaction sphere of radius $6a$. Indeed, the interaction forces between particles at a larger distance are negligible. This leads to a significant reduction in calculation time.

The DLVO interaction force is given by the sum of the Van der Waals attraction force $\overrightarrow{F_{ij\,VdW}}$ and of the electrical repulsion force $\overrightarrow{F_{ij\,el}}$ that are

$$\overrightarrow{F_{ij\,VdW}} = -\frac{A_H}{6}\left(\frac{4a^2}{r^3} - \frac{4a^2 \cdot r}{\left(r^2 - 4a^2\right)^2} + \frac{8a^2}{r^2 \cdot \left(r^2 - 4a^2\right)}\right) \tag{4}$$

and

$$\overrightarrow{F_{ij\,el}} = -\frac{64\,\pi \cdot k_B \cdot T \cdot n_{ion} \cdot a}{\kappa} \cdot \gamma_G^2 \cdot e^{(-\kappa \cdot (r-2a))} \tag{5}$$

A_H is the Hamaker constant which is $3.7 \cdot 10^{-20}$, and γ_G is a function of the surface potential Ψ_0 according to the relationship

$$\gamma_G = \tanh \frac{e\Psi_0}{4k_B \cdot T} \tag{6}$$

$\overrightarrow{F_i^R}$ is the random Langevin force (accounting for Brownian motion)

$$\overrightarrow{F_i^R} = \sqrt{2 \cdot k_B \cdot T} \cdot \overrightarrow{W_v} \tag{7}$$

where $\overrightarrow{W_v}$ is a random vector whose components are independent Gaussian random numbers with zero mean and unit variance.

$\overrightarrow{F_i^D}$ is the viscous drag force (Stokes law)

$$\overrightarrow{F_i^D} = -6 \cdot \pi \cdot \mu \cdot a \cdot \overrightarrow{v_i} \tag{8}$$

which depends on the viscosity of the medium µ, on the velocity of the particle $\overrightarrow{v_i}$ and on the particle radius a.

A semi-implicit finite differences method was used for numerical integration [17]. To ensure robustness when the particles are close to each other (the DLVO potential tends to $-\infty$ when the particles are in contact), a contact force was added when two particles were at a distance lower than $2a$which was modeled as a Hertz contact force [18].

In order to approach the behavior of an infinite medium, periodic boundary conditions were implemented [19]. At time 0, a minimum interparticle distance of 1 nm is imposed. A ionic strength of 0.005 M and a surface potential of 1 mV, which is characteristic of conditions close to the point of zero charge, are considered, that is of a zeta potential 0 mV [20].

3.2. Gyration radius and fractal dimension

When the positions of all the spheres at a given time instant are known, it is possible to compute the gyration radius R_{gyr} and the fractal dimension d_f of the agglomerates [21]

$$d_f = \frac{\log\left(\frac{\xi}{k_f}\right)}{\log\left(\frac{R_{gyr}}{a}\right)} \tag{9}$$

where ξ is the number of primary particles (spheres of 40 nm radius) that constitute the aggregate and k_f is the fractal pre-factor [22] which is considered equal to 1.2 [14].

R_{gyr} is given by the geometrical average distance between the spheres'centers and the agglomerate center of mass. The formula used by Filippov et al. [23] also contains the radius of the primary particle a, so that for $\xi \to 1, R_{gyr} \to a$:

$$R_{gyr}^2 = \frac{1}{\xi}\sum_{i=1}^{\xi}\left[\left(x_i - x_g\right)^2 + \left(y_i - y_g\right)^2 + \left(z_i - z_g\right)^2 + a^2\right] \tag{10}$$

where the coordinates of the centers of the spheres are x_i, y_i and z_i and the coordinates of the agglomerate center of mass are x_g, y_g and z_g:

$$x_g = \frac{\sum_i^{\xi} x_i}{\xi} \tag{11}$$

$$y_g = \frac{\sum_i^{\xi} y_i}{\xi} \tag{12}$$

$$z_g = \frac{\sum_i^{\xi} z_i}{\xi} \tag{13}$$

3.3. Population balance model

The population balance equation was used to describe the evolution of large colloidal boehmite systems in terms of size distribution and number of primary particles 10^{21}.

The governing equation was solved in its discrete form

$$\frac{dN_k}{dt} = \frac{1}{2}\sum_{i=1}^{k-1} \beta_{i,k-i}^{agg} N_i N_{k-i} - N_k \sum_{i=1}^{\infty} \beta_{ik}^{agg} N_i \tag{14}$$

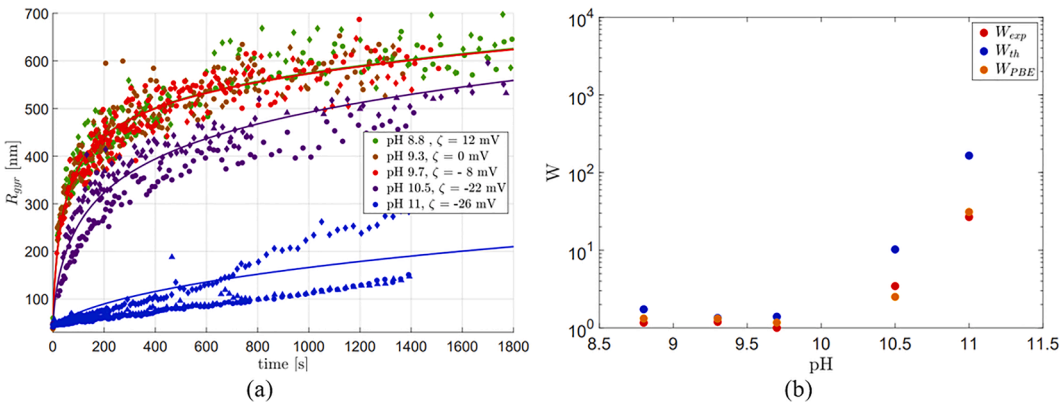

Fig. 2. (a) Evolution of average hydrodynamic intensity radius, measured with DLS on a Pural SB3 suspension of 0.04 g/L and different pH. The solid lines are the result of the population balance model while the dots represent the experimental results. Here, different symbols (●, ◆ and ▲) correspond to duplicate tests. (b)Fuchs stability ratio: comparison between theoretical [10], experimental [27] and the population balance value.

where

- N_k is the concentration number of clusters of mass ξ_k, where the mass is the number of primary particles constituting the aggregate k;
- the first term represents all possible collisions leading to the formation of an aggregate of mass ξ_k;
- the second term represents the rate of disappearance of the aggregates of mass ξ_k due to aggregation with aggregates of any mass;
- the β terms are Brownian agglomeration kernels;

$$\beta_{ij} = \frac{2}{3}\frac{k_B T}{\eta W}\left(\xi_i^{\frac{1}{df}} + \xi_j^{\frac{1}{df}}\right)\left(\xi_i^{-\frac{1}{df}} + \xi_j^{-\frac{1}{df}}\right); \tag{15}$$

The number of primary particles in each agglomerate was related to the agglomerate fractal dimension via the relationship in Eq.(9).

The population balance parameters that were adjusted with DLS data are the Fuchs coefficient W and the parameters of the curve $d_f = f(R_{gyr})$. For this latter, an arctangent function was used to reproduce the shape obtained from the Lagrangian simulation. However, the parameters of this function were adjusted with experimental data, because Lagrangian simulation is impacted by the low number of particles and by the assumption of periodic conditions involving agglomerates breakage.

Before adjusting the model kernels with DLS data, it was necessary to consider the maximum radius that could be measured with DLS as well as the type of weighting to compute the average agglomerate radius. Since the maximum radius that can be measured experimentally via DLS with our device is 1.5 μm, such radius was considered as the threshold R_{gyr}^{lim} for the "cut" of the population balance size distribution. This entailed a limit mass number of

$$\xi_{lim} = k_f \cdot \left(\frac{R_{gyr}^{lim}}{a}\right)^{df} \tag{16}$$

where k_f is the fractal pre-factor (assumed equal to 1.2 [24]) and a is the radius of the primary particle. The cut population is composed by all the agglomerates that have a mass number ξ such that

$$\xi \leq \xi^{lim}. \tag{17}$$

Afterwards it is necessary to estimate a weighted average radius considering that DLS measures an effective diffusion coefficient based on how quickly the intensity of the scattered light changes. The diffusion coefficient is then related to the average radius R_{gyr} via the Stokes-Einstein law

$$D = \frac{k_B \cdot T}{6 \cdot \pi \cdot \mu \cdot R_{gyr}}. \tag{18}$$

Considering the effective scattering coefficient D_{eff} described by Sun et al. [25]

$$D_{eff} \simeq \frac{\int_0^\infty R_{gyr,i}^6 \cdot D_i \cdot G_i \cdot dR_{gyr}}{\int_0^\infty R_{gyr,i}^6 \cdot G_i \cdot dR_{gyr}} \tag{19}$$

where R_{gyr}, D_i and G_i are the gyration radius, the diffusion coefficient and the number distribution of particles of the class i.

By substituting D_i with the Stokes-Einstein law. Eq.(19) in a discretized form becomes

$$D_{eff} \simeq \frac{\sum_{i=1}^{n_{class}} R_{gyr,i}^6 \cdot D_i \cdot N_{p,i}}{\sum_{i=1}^{n_{class}} R_{gyr,i}^6 \cdot N_{p,i}} \tag{20}$$

where $N_{p,i}$ is the number of agglomerates belonging to the class i.

According to the Stokes-Einstein law the average radius $\overline{R_{gyr}}$ is related to the effective diffusion coefficient

$$\overline{R_{gyr}} \simeq \frac{6\pi \cdot \mu}{k_B \cdot T \cdot D_{eff}}. \tag{21}$$

Substituting Eq.(20) in Eq.(21) leads to

$$\overline{R_{gyr}} \simeq \frac{\sum_{i=1}^{n_{class}} R_{gyr,i}^6 \cdot N_{p,i}}{\sum_{i=1}^{n_{class}} R_{gyr,i}^5 \cdot N_{p,i}}. \tag{22}$$

which is the average weighted radius consistent with the DLS principle.

The algorithm of Levenberg-Marquardt was used to adjust the parameters of the population balance model in order to represent DLS data, these parameters are W and the parameters of the $d_f = f(R_{gyr})$ relationship.

3.4. Morphological model

The morphological aggregation model [14] relies on a sequential aggregation of primary objects. It enables to tune the compactness of the final assemblies according to the probability of sticking the primary objects either in the concave points or in concave points close to the center of mass of the assembly. In the case of identical spherical primary objects, a specific numerical scheme enables to build assemblies of several millions of primary objects. With the purpose of building the agglomerates within the size range predicted by the population balance, a resolution of 35 nm^2/voxel was considered. A discretized agglomerates mass distribution was built from the solution of the population

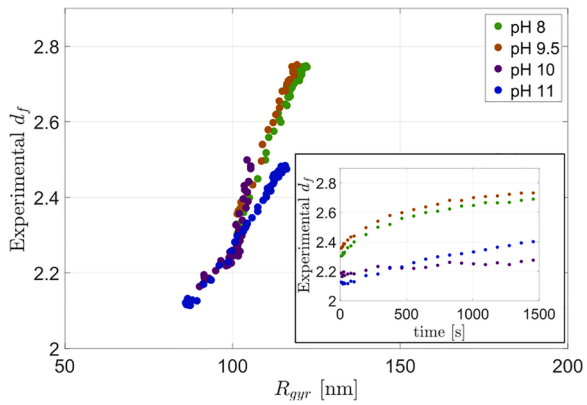

Fig. 3. Experimental SAXS data acquired following the agglomeration process of a boehmite powder at 5 g/L, for a pH increase from 8 to 10.

balance equation. The agglomerates belonging to such distribution were used as primary agglomerates to make an agglomerate of agglomerates, respecting the distribution [26].

4. Results

4.1. Experimental study of boehmite agglomeration in aqueous suspension

Boehmite suspensions initially peptized at pH 3 contain essentially assemblies of few tens of nm. Such objects are considered in this work as primary aggregates. It was observed by image analysis of STEM micrographs (see Appendix B) that the agglomerates formed by bringing the pH closer to the PZC can be re-dispersed again in the same primary aggregates if the pH is decreased down to 3. Therefore, the agglomeration phenomenon is reversible and is qualitatively in agreement with DLVO theory, considering the coagulation of identical primary particles.

The evolution of the agglomerates average gyration radius measured with DLS is reported, for different pH, in Fig. 2a. The dots represent the experimental results while the lines are the result of the population balance which will be discussed in paragraph 4.3.

The noise on the measurement becomes more significant with increasing polydispersity caused by agglomeration. For this reason, it was necessary to repeat each experiment several times in order to have a reliable data set.

The pH affects the zeta potential ζ of the suspended particles, which is zero when the pH is 9.3 (as expected for boehmite suspensions [28]). It can be noted that the closer the pH is to the Point of Zero Charge (PZC), the more agglomeration is favored. This is in agreement with the DLVO theory because if the zeta potential decreases, the repulsion forces also decrease. Van der Waals forces of attraction, on the contrary, do not depend on pH and are always present.

In Fig. 2b we find the value of Fuchs *W*using the theoretical formula in Eq.(1) and the experimental values computed according to Holthoff *et al.* [27] (details on the computation are in Appendix A).

According to a preliminary study of the ζ potential and of the titration curve of the boehmite suspensions, the ζ potential is almost not affected by a pH change within the range 3–8. Therefore, to destabilize the suspension and observe agglomeration the pH has been tuned in the

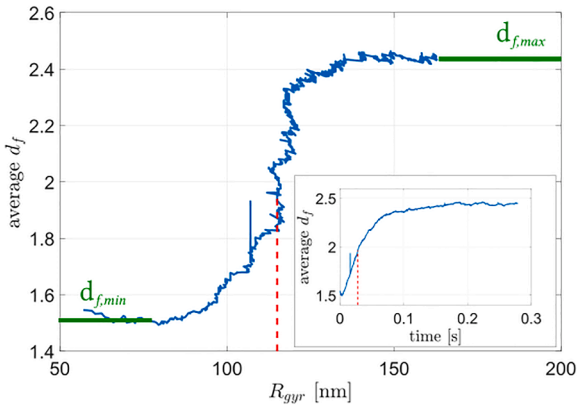

Fig. 5. Illustration of the phase diagram and of the parameters of the Eq. (23). The evolution of the average fractal dimension over 0.3 s is reported in the right corner.

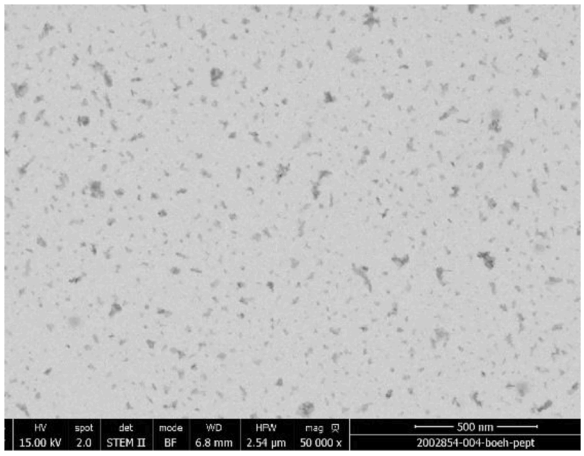

Fig. 6. STEM image of the aggregates of a peptized boehmite suspension with pH 3.5.

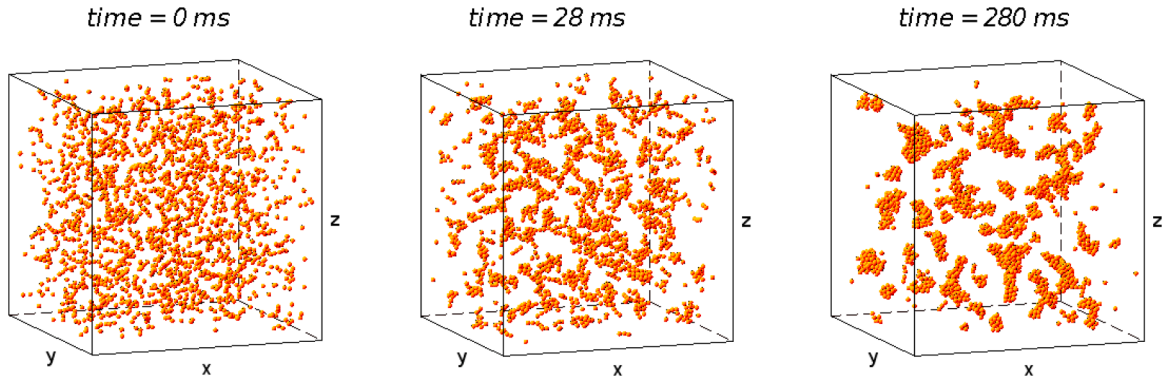

Fig. 4. Configuration of the agglomerates system inside the cubic control volume of length 3800 nm at different time instants, simulated with Brownian dynamics model. x, y and z are the volume coordinates.

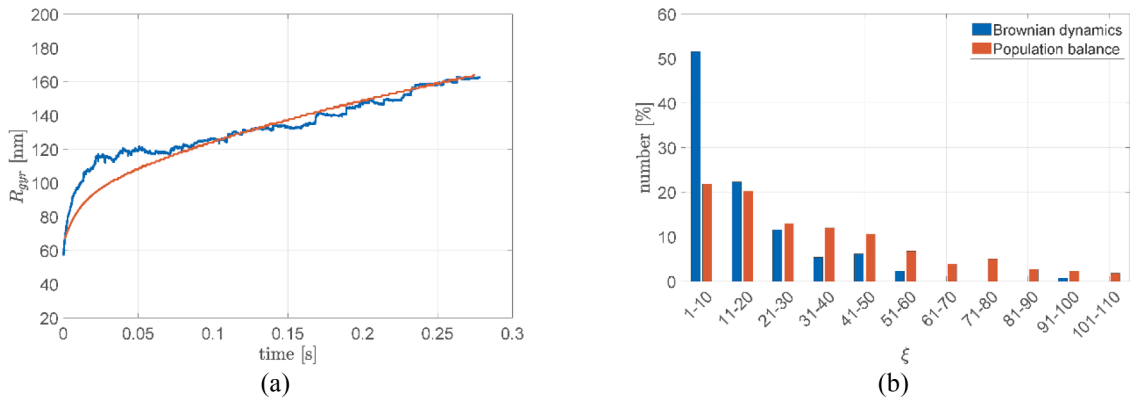

Fig. 7. Comparison between the Lagrangian simulation and the population balance in terms of average diameter evolution (a) and final mass distribution (b) after 0.278 s.

Table 1
Adjusted parameters of the population balance model.

pH	8.8	9.3	9.7	10.5	11
$d_{f,2}$	2.75	2.75	2.75	2.85	/
R_{cut}	600	596	607	600	/
a_a	3.96	3.97	2.69	1.80	/
W_{PBE}	1.32	1.32	1.17	2.50	31.14

range 8.8–11.

The DLS results for pH within the range 8.8 - 9.7 are similar, leading to a quite fast growth of the average hydrodynamic radius. Indeed, these conditions are close to the point of zero change (PZC). At pH 10.5 and at pH 11 the agglomeration is slower but still visible within 20 min.

For a pH within 8.8 and 10.5, all the experimental points show an initial rapid growth, followed by a slower one. This regime change has a twofold explanation. First, R_{gyr} evolution is dependent on the change in fractal dimension: at the beginning of the agglomeration process the fractal dimension is small, so the structures formed tend to be linear; at the end of the process, the fractal dimension is high, so more compact structures are produced.

In second place, kinetics slows down with time as the amount of small, isolated aggregates decreases. The transition between the two regimes occurs once R_{gyr} exceeds a certain value. For pH between 8.8 and 10.7, this limit is reached within the 20 min experiment due to rapid agglomeration, favored by low electrostatic repulsion forces near PZC. At pH 11 the repulsion forces are higher, and agglomeration follows a slow linear growth, without reaching the threshold size for the regime transition.

The high experimental variability of the mean radius can be due to several factors. First, the low boehmite concentration, necessary to observe slow kinetics, decreases the signal-to-noise ratio. In addition, the necessity of maintaining Brownian conditions imposed that the suspensions were not mixed after the ammonia injection, this may lead to local pH variations that can influence the agglomeration in the first few seconds leading to different slope in the initial linear growth.

Additional information can be extracted from the results of the SAXS analysis, where the scattering curves were interpreted with the Beaucage model using the method adopted by Speyer et al. [29].

Since the coagulation observed for these experiments may be affected by the shear (necessary to ensure continuous sampling), the SAXS results are not directly used for the study of agglomeration kinetics in Brownian motion. But they highlight that, during the agglomeration, a relationship exists between fractal dimension and gyration radius

Table A1
Results of the estimation of the initial dimerization constant and of the Fuchs stability ratio.

pH	8.8	9.3	9.7	10.5	11
$k_{11} \cdot \xi_0$	139	135	161	47	6
W_{exp}	1.16	1.19	1.00	3.45	26.75

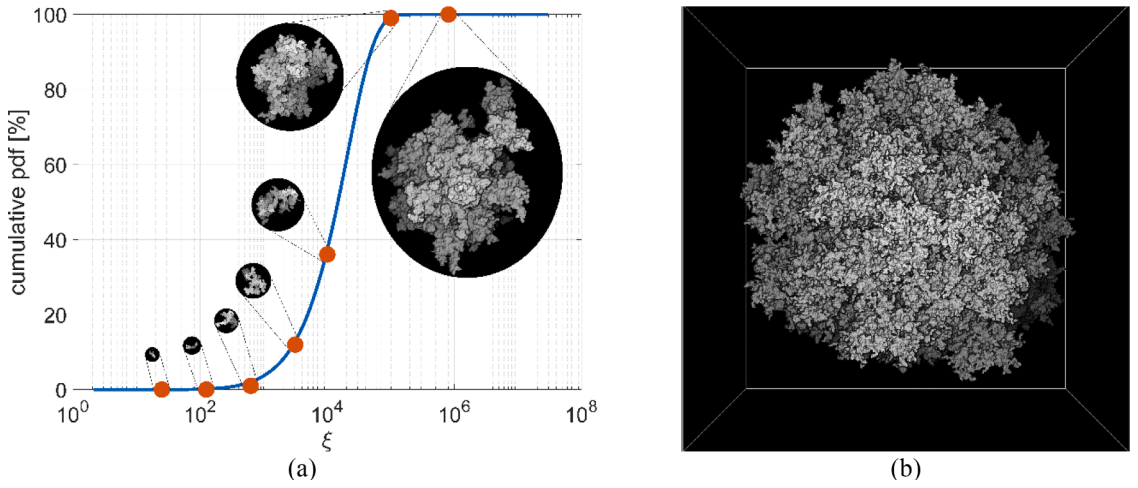

Fig. 8. (a)Cumulate probability density function obtained from a population-balance simulation. The operating conditions are pH = 9.6 and 1 g/L, the time simulated is of one hour. The seven agglomerates of the discrete distribution are also represented. (b)Simulated morphology of a boehmite dried powder after agglomeration within a colloidal suspension at 1 g/L ad PZC.

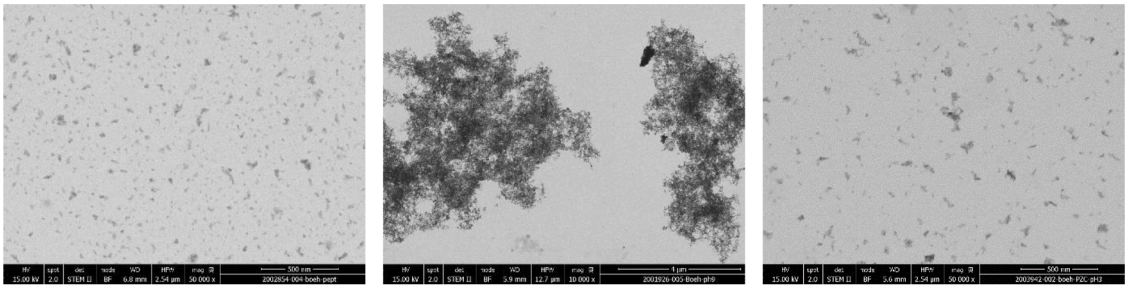

Fig. A1. STEM images of the suspensions A (a), B(b) and A'(c).

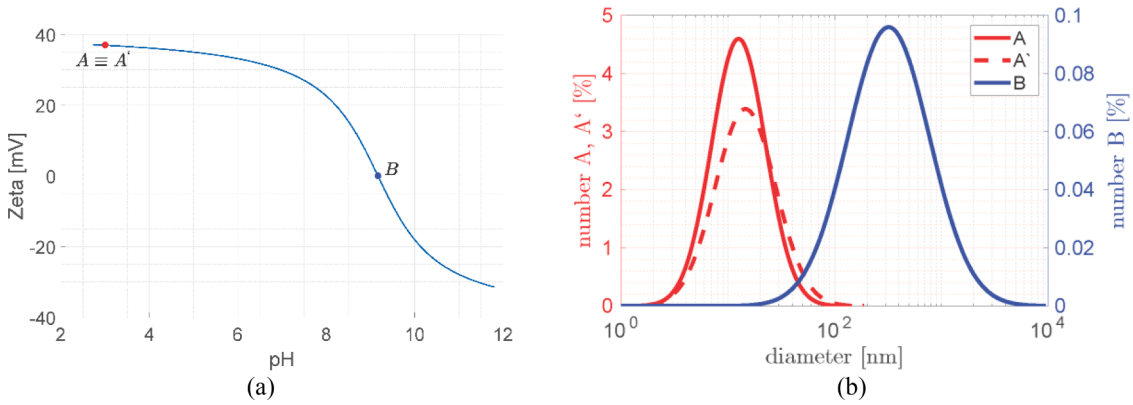

Fig. A2. Zeta potentials and size distribution obtained with STEM image analysis.

(Fig. 3).

These results are related to the size limits of the analysis and the approach used for the interpretation of the SAXS curves. In this regard, it is to be noted that our results refer to agglomerates whose gyration radius is between 50 and 150 nm.

A quasi-linear trend can be observed in the phase diagram. This may be due to a different agglomeration mechanism in the initial instants of the process, since for all pH values, after an initial growth phase the size and fractal dimension tend to stabilize.

The relationship between agglomeration kinetics and structure (d_f) is still an open question and offers an interesting perspective for further experimental investigation. According to the literature on diffusion and reaction limited aggregation mechanisms [30,31] fast assembly kinetics (close to PZC) lead to loose structures with a low fractal dimension, whereas slower kinetics (far from PZC) produce more compact structures and thus a higher d_f. However, the behavior of the boehmite agglomerates is the opposite, as also confirmed by the SAXS results and the STEM images of these samples [24]. This can be due to the presence of two agglomeration phases, where possibly rearrangement occurs once a certain R_{gyr} is exceeded. It would be interesting to study whether the relationship between kinetics and d_f changes with the size of the objects undergoing agglomeration. The relationships expected from the literature could be met on the small scale of aggregates (up to a few tens of nm), as opposed to those observed for agglomerates in this work.

4.2. Comparison between population balance and Brownian dynamics model

The agglomeration of identical primary spherical aggregates was simulated using a Lagrangian Brownian-DLVO model. Initial conditions of a colloidal peptized mixture with pH 3 and zeta potential 35 mV are assumed. The system is perturbed by an increase in pH and a decrease in zeta potential to 1 mV (to simulate the point of zero charge).

During the first instants of the agglomeration process, particles tend to form linear agglomerates, before undergoing a rearrangement that increases their fractal dimension. This is illustrated by the Brownian-DLVO simulations (Fig. 4) showing the evolution of the agglomerate's arrangement with time.

The fractal dimension evolution with respect to the average agglomerate gyration radius is reported in the phase diagram obtained from the Brownian-DLVO simulations in Fig. 5, in the corner it is also reported the evolution of the average fractal dimension, which increases linearly with time in the first instants and stabilizes afterwards.

It can be assumed that the fractal dimension and the gyration radius respect a relationship of the type

$$d_f = d_{f,1} + \left(d_{f,2} - d_{f,1}\right) \cdot \frac{arctan\left(a_a \cdot \frac{R_{gyr} - R_{cut}}{R_{cut}}\right) + \frac{\pi}{2}}{\pi} \tag{23}$$

which can represent the two plateaus of Fig. 5 by means of the following parameters:

- a_a related to the slope of the d_f function;
- R_{cut} corresponding to the abscissa of the inflection point, is the cutoff gyration radius;
- $d_{f,1}$ and $d_{f,2}$ are two parameters that, together with a_a determine the value at the two plateaus $d_{min}$and d_{max}.If $a_a > 20$ then $d_{f,1} \simeq d_{min}$ and $d_{f,2} \simeq d_{max}$.

This shape is the result of the physical interactions between the particles leading first to agglomeration and then to rearrangement. The fractal dimension of the lager cluster is relatively high with respect to literature diffusion and reaction limited aggregation processes due to flexible bonds, which enable the assemblies to twist and fold. The results of the simulations were used to describe the shape of the $d_f = f(R_{gyr})$ function and to gain a qualitative insight into agglomeration mechanisms, especially for fast kinetics that are difficult to measure experimentally. The fractal dimension and size results, however, cannot be

directly compared with the experimental results, as 2048 primary particles may not be sufficient to represent a real system.

The fact that the fractal dimension evolves with the size of the agglomerate during agglomeration has also been observed with SAXS analysis as it is reported in Fig. 3. The experimental curve cannot represent the two plateaus since the initial primary particle and the final agglomerate are out of the measurement size limits. In addition, the non-spherical geometry of the primary particle, as it can be observed in Fig. 6, may have an impact on the agglomerate fractal dimension, which can explain the difference between the d_f simulated by the Brownian Dynamic model and the one measured with SAXS analysis.

By fitting the phase diagram obtained from Brownian-DLVO simulations with Eq.(23) the results obtained for $d_{f,1}$ and $d_{f,2}$ are 1.53 and 2.48 respectively, a_a is 25.69 and R_{cut} is 115 nm. These parameters have been used to model the d_f and R_{gyr} relationship of the population-balance model. Using the particle size and concentration of the Brownian Dynamics model. Fig. 7a shows the comparison between the two models concerning the evolution of the average gyration radius, while Fig. 7b shows the cluster mass distribution at the time 0.278 ms.

The Brownian Dynamics and the Population Balance model are in agreement for $W = 1.7$. This value is close to 1 when the pH of the suspension is close to the PZC, and it is highly sensitive to small varitions of pH.

Therefore, the Fuchs coefficient is still in the order of magnitude estimated for these conditions. It is experimentally challenging to measure a Fuchs stability ratio and small variations are acceptable if W remains within the right order of magnitude. As a result, the population balance respects the time scale of the coagulation simulated via Brownian dynamics. The discrepancies of the mean gyration radius between 0 and 0.05 s can be explained by the fact that the Lagrangian simulation accounts only for 2048 particles. Indeed the Brownian dynamics is less statistically representative of a real colloidal system with respect to the population balance model.

4.3. Adjusting population balance parameters with DLS results

The result of the population balance are the lines reported against experimental dots in Fig. 2a. It can be noted that the model can represent the experimental data. The Table 1 reports the parameters obtained for the different DLS experiments. All the data were compared with the population balance model using a $d_{f,1}$ of 1.5, while $d_{f,2}$ and R_{cut}vary within a narrow range. In particular, a $d_{f,2}$ of 2.75 - 2.8 results in very dense assemblies at the end of the agglomeration process. This agrees with the results of image analysis of STEM micrographs of boehmite suspensions near PZC, where a fractal dimension of about 2.8 was estimated [24].

The parameter that has the highest impact on the population balance result is the Fuchs stability ratio W_{PBE}. Indeed, for the data set at pH 11, for which $W_{PBE} = 31.14$, the agglomeration kinetic is independent of the values of all the other parameters. W_{PBE} is always between the theoretical and the experimental Fuchs stability ratio as shown in Fig. 2b.

The comparison between the population balance and the DLS data obtained at low boehmite concentration enables to set ranges for the parameters of the model, which make it capable to represent evolution of suspensions at higher concentration.

In order to approach the boehmite concentration of the manufacturing process the population balance was extrapolated at a concentration of 1 g/L and at PZC. Fig. 8a shows the mass cumulative distribution after an agglomeration process of 1 h, when it is assumed that the colloidal system has reached the equilibrium size distribution. This result has been used to adjust a morphological model of a powder obtained by drying the suspension.

The model only simulates the final state without describing the kinetics of agglomeration or re-arrangement, the primary aggregates (approximated by spheres) are rigidly bound together. The final morphology predicted by the population balance model is built using the mass distribution and the $d_f(\xi)$ function, considering that $R_{gyr}$is related to mass via Eq.(9). The morphological model [14] can be used iteratively to form clusters of spheres as primary objects, leading to a high fractal dimension. However, the fast simulation scheme for spheres as primary objects only, is then no longer possible, limiting the exploration of the figures.

With the aim of reducing the computation time, we considered 100 agglomerates belonging to a discretized cumulative distribution of seven classes (red points in Fig. 8a) with a number of primary particles ranging from 25 to $81 \cdot 10^5$. The fractal dimension of these agglomerates is computed with the adjusted $d_f(\xi)$ relationship, and it takes a value of 1.70 for the smaller agglomerates and of 2.82 for the larger ones.

The coagulation of the agglomerates has been simulated via the morphological model [14] using the maximum compactness parameters. An illustration of the morphology of the final dry powder is shown in Fig. 8b.

5. Conclusion

Boehmite agglomeration phenomenon is extremely chaotic and involves assembly at multiple size scales, from a few tens of nanometers to several microns. The use of multi-technique characterizations highlights structural properties at different scales. A strategy has been developed for generating the 3D morphology of a boehmite grain after agglomeration in a colloidal suspension.

Our contribution consists in describing a system that evolves according to physical-chemical parameters using structural parameters like size distribution, fractal dimension and order of assembly. The final microstructure is generated with an aggregation morphological model where different sticking probabilities are assigned on concave and non-concave points of a cluster. To relate these probabilities to physical-chemical parameters, two physical models have been used: a Lagrangian Brownian dynamics model and a population balance model. The first one provided information about the relationship between fractal dimension and agglomerate mass ξ. The second one enables to simulate a realistically large colloidal system. Since the relationship found with the first model can also be confirmed by SAXS analysis results, the function $d_f(\xi)$ has been implemented in the Smoluchowski kernel of the population balance model.

DLS experimental results have been used to adjust the kernel parameters. The size distribution and the fractal dimension obtained from the population balance was finally used to parameterize the morphological model and to build an agglomerate of agglomerates.

The experimental DLS results are qualitatively in agreement with the DLVO theory, indeed the closer the pH to the point of zero charge, the faster the agglomeration process is.

The resistance to agglomeration has been quantified via the Fuchs stability coefficient. A good agreement has been found between the experimental, the theoretical and the adjusted Fuchs coefficient of the Smoluchoswki kernel.

In order to relate the morphology of an agglomerate to the conditions of agglomeration, experimental methods and models of agglomeration dynamics are often compared and inter-combined [32,33] or a stochastic agglomeration model is parameterised using experimental data [5]. In this study, it has been proposed to use all these approaches, and in particular to use the population balance as a bridge between the experimental results and the morphological model of agglomeration.

This work has made it possible to highlight many prospects for improvement, like implementing a Brownian model with non-spherical particles, which may have an impact on the parameters of the $\xi(d_f)$ function. In addition, the natural perspective of this work is to consider boehmite crystallites as primary particles rather than aggregates. This would enable the simulation of the textural properties like pores distribution and tortuosity [34]. Then, taking into account the inclusion of shear-induced agglomeration and breakage to higher concentrations, will approach the industrial operating conditions of the manufacturing

process of the support.

In order to innovate catalytic materials, it would be useful to simulate the impregnation process on the modelled morphology, with the possibility of relating the agglomeration pH to the dispersion of active sites on the final solid [35] and use the morphological model to feed a pore network model [36] to relate manufacturing process and textural and transport properties within a catalytic support.

Declaration of Competing Interest

The authors declare that they have no known competing financial interests or personal relationships that could have appeared to influence the work reported in this paper.

Data availability

Data will be made available on request.

Acknowledgements

DLS experiments were realized with the resources and equipment provided by IFP energies nouvelles.

SAXS experiments were performed on the SWING beamline at SOLEIL Synchrotron, France. We are grateful to Thomas Bizien for assistance and to the SOLEIL staff for smoothly running the facility.

Appendix A. Computation of experimental Fuchs coefficient

According to Holtoff *et al.* [27], the Fuchs stability coefficient can be computed at a time t close to 0 assuming that only dimers have formed. For dynamic light scattering the dimerization kinetic constant can be approximated

$$k_{11} \simeq \frac{1}{\xi_0}\cdot\frac{R_2}{R_2 - R_1}\cdot\left(\frac{\frac{dR(t)}{dt}|_{t\to 0}}{R(0)}\right) - \left(\frac{\frac{dI(q,t)}{dt}}{I(q,0)}\right) \tag{A.1}$$

where:

- R_1 and $R_2$are the hydrodynamic radius of the monomer and dimer respectively;
- $I(q, t)$ is the scattered intensity at scattering vector q and at time t;
- a is the radius of the primary particles;
- ξ_0 is the initial particle number concentration.

The stability ratio can be estimated by dividing the fast coagulation rate constant k_f by a slow coagulation rate constant k_s[37]

$$W = \frac{k_{11,fast}}{k_{11,slow}} \tag{A.2}$$

From the experimental data the average fitting curves shown have been calculated using the following functions

- from pH 8.8 to pH 10.5

$$R(t) = A\cdot\log(t)^2 + B\cdot\log(t) + C \tag{A.3}$$

- for pH 11

$$R(t) = D\cdot\exp(E\cdot t) \tag{A.4}$$

k_{11}has been estimated with the following hypotheses:

- The derivative of the scattered intensity is negligible with respect to the hydrodynamic radius one, such assumption relies on the fact that the boehmite suspension has a low concentration, entailing a weak scattered light intensity

$$\left(\frac{\frac{dI(q,t)}{dt}}{I(q,0)}\right) \ll \frac{1}{\xi_0}\cdot\frac{R_2}{R_2 - R_1}\cdot\left(\frac{\frac{dR(t)}{dt}|_{t\to 0}}{R(0)}\right) \tag{A.5}$$

- The lowest acquisition time with DLS device is 20 s, we assume that at this time only dimers are present. Therefore we call $R_2 = R(20s)$.

Table A1 reports the results for the experiments at 0.04 g/L of Pural SB3.

Appendix B. Aggregates and agglomerates

It has been observed via STEM image processing that the agglomerates formed by approaching the pH to PZC can be re-dispersed into the same initial aggregates if the pH is brought close to the initial acid one (pH 3). Three colloidal suspensions have been prepared with 0.02 g/L of Pural SB3 and have been characterized with STEM:

- **A**: The initial suspension with pH close to 3;
- **B**: Ammonia has been added to the suspension **A** in order to reach a pH close to PZC;
- **A'**: Acid has been added to the suspension **B** with the purpose of decreasing the pH to 3, the same of suspension **A**.

The STEM images of the three suspensions are in Fig. A1a, A1b and A1c.

The zeta potentials of these suspensions are illustrated in Fig. A2a while the size distributions computed via STEM image processing are in Fig. A2b.

It can be observed that and increase in pH towards PZC increases considerably the size of colloidal boehmite due to the decrease of the electrostatic repulsion forces [10].

When the pH is decreased again to 3, the size of the colloids decreases. The size distribution of the objects in **A** and in **A'** are nearly the same, with a relatively thin size distribution.

The image processing also revealed that the fractal dimension of **A** and **A'** are the same, being equal to 2.69 and 2.66 respectively [24].

This means that the agglomerates can be peptized into the primary initial aggregates, these latter cannot be modified by the sole acid injection (within a concentration range that does not imply boehmite dissolution or ionic strength-induced coagulation).

In conclusion, the agglomeration of colloids of the initial suspension can be seen as the coagulation of primary particles (the aggregates). These particles remain unchanged both in terms of size and structure. The reversibility of the agglomeration phenomenon is then qualitatively in agreement with the DLVO theory and the agglomeration can be modelled considering the reversible coagulation of identical primary particles.

References

[1] D. Chiche, M. Digne, R. Revel, C. Chanéac, J.-.P. Jolivet, Accurate determination of oxide nanoparticle size and shape based on X-ray powder pattern simulation: application to boehmite AlOOH, The J. Phys. Chem. C 325 112 (23) (2008) 8524–8533.

[2] P. Euzen, P. Raybaud, X. Krokidis, H. Toulhoat, J. Le Loarer, J. Jolivet, C. Froidefond, Alumina, in Handbook of Porous Solids, Wiley, 2002. Ch. 4.7.2.

[3] G. Nichols, S. Byard, M.J. Bloxham, J. Botterill, N.J. Dawson, A. Dennis, V. Diart, N.C. North, J.D. Sherwood, A review of the terms agglomerate and aggregate with a recommendation for nomenclature used in powder and particle characterization, J. Pharmaceutical Sci. 91 (10) (2002) 2103–2109.

[4] L.M. Anovitz, X. Zhang, J. Soltis, E. Nakouzi, A.J. Krzysko, J. Chun, G.K. Schenter, T.R. Graham, K.M. Rosso, J.J. De Yoreo, A.G. Stack, M. Bleuel, C. Gagnon, D.F. R. Mildner, J. Ilavsky, K. I, Effects of ionic strength, salt, and ph on aggregation of boehmite nanocrystals: tumbler small-angle neutron and x-ray scattering and imaging analysis, Langmuir: The ACS J. Surfaces and Colloids (2018).

[5] E. Nakouzi, J.A. Soltis, B.A. Legg, G. Schenter, X. Zhang, T. Graham, K.M. Rosso, L. M. Anovitz, J.J. de Yoreo, J. Chun, Impact of solution chemistry and particle anisotropy on the collective dynamics of oriented aggregation, ACSnano 12 (10) (2018) 10114–10122.

[6] M. Hütter, Local structure evolution in particle network formation studied by brownian dynamics simulation, J. Colloid Interface Sci. 231 (2) (2000) 337–350.

[7] S. Kumar, D. Ramkrishna, On the solution of population balance equations by discretization - i: fixed pivot technique, Chem. Eng. Sci. 8 (8) (1996) 1311–1332.

[8] M.V. Smoluchowski, ber brownsche molekularbewegung unter einwirkung uerer krfte und deren zusammenhang mit der verallgemeinerten diffusionsgleichung, Electrische Endosmose und Strmungsstrme (1921) 204–210.

[9] M. Lattuada, A. Zaccone, H. Wu, M. Morbidelli, Population-balance description of shear-induced clustering, gelation and 345 suspension viscosity in sheared dlvo colloids, Soft Matter 12 (24) (2016) 5313–5324.

[10] E.J. Verwey, J.T.G. Overbeek, Theory of the Stability of Lyophobic colloids: the Interaction of Sol Particles Having an Electric Double Layer, Elsevier publishing company Inc., 1948.

[11] H. Hamaker, The london-vander waals attraction between spherical particles, Physica IV 10 (1937) 1058–1072.

[12] P. Langevin, Sur la thorie du mouvement brownien, Comptes-Rendus de l'Acadmie des Sci. (1908).

[13] P.C. Hiemenz, R. Rajagopalan, Principles of Colloid and Surface Chemistry, Marcel Dekker Inc, 1986.

[14] G. Ferri, S. Humbert, M. Digne, J.-.M. Schweitzer, M. Moreaud, Aggregation morphological model with variable compactness: application to colloidal system, Image Anal. and Stereol. 40 (2) (2021) 71–84.

[15] R. Pecora, Dynamic Light scattering: Applications of Photon Correlation Spectroscopy, Plenum press, New York, 1985.

[16] G. Beaucage, D.W. Schaefer, Structural studies of complex systems using small-angle scattering: a unified guinier/power law approach, J. Non Cryst. Solids 172-174 (1994) 797–805.

[17] G. Volpe, G. Volpe, Simulation of a brownian particle in an optical trap, Am. J. Phys. 81 (3) (2013) 224–230.

[18] P.A. Cundall, O.D.L. Strack, A discrete numerical model for granular assemblies, Gotechnique 29 (1) (1979) 47–65.

[19] W. Yang, Z. Zhou, D. Pinson, A. Yu, Periodic boundary conditions for discrete element method simulation of particle flow in cylindrical vessels, Ind. Eng. Chem. Res. 53 (19) (2014) 8245–8256.

[20] G.V. Lowry, R.J. Hill, S. Harper, A.F. Rawle, C.O. Hendren, F. Klaessig, U. Nobbmann, P. Sayre, J. Rumble, Guidance to improve the scientific value of zta-potential measurements in nanoehs, Environ. Sci.: Nano 3 (5) (2016) 953–965.

[21] L. Gmachowski, Mass–radius relation for fractal aggregates of polydisperse particles, Colloids and Surfaces A: Physico Chem. Eng. Aspects 224 (1–3) (2003) 45–52.

[22] C.M. Sorensen, G.C. Roberts, The prefactor of fractal aggregates, J. Colloid Interface Sci. 186 (CS964664) (1997) 447–452.

[23] A.V. Filippov, M. Zurita, D.E. Rosner, Fractal-like aggregates: relation between morphology and physical properties, J. Colloid Interface Sci. 229 (1) (2000) 261–273.

[24] G. Ferri, S. Humbert, J.-.M. Schweitzer, M. Digne, V. Lefebvre, M. Moreaud, Mass fractal dimension from 2d-microscopy images via an aggregation model with variable compactness, J. Microsc. 286 (1) (2021).

[25] Y. Sun, Investigating diffusion coefficient using dynamic light scattering technique, arXiv:Phys. (2018).

[26] L. Pereira de Oliveira, J.J. Verstraete, M. Kolb, A monte carlo modeling methodology for the simulation of hydrotreating processes, Chem. Eng. J. 207–208 (2012) 94–102, 375.

[27] H. Holthoff, S.U. Egelhaaf, M. Borkovec, P. Schurtenberger, H. Sticher, Coagulation rate measurements of colloidal particles by simultaneous static and dynamic light scattering, Langmuir 12 (1996) 5541–5549.

[28] M. Kosmulski, ph-dependent surface charging and points of zero charge. iv. update and new approach, J. Colloid Interface Sci. 337 (2) (2009) 439–448.

[29] L. Speyer, S. Humbert, T. Bizien, V. Lecocq, A. Hugon, Peptization of boehmites with different peptization index: an electron microscopy and synchrotron small-angle x-ray scattering study, Colloids and Surfaces A: Physicochem. Eng. Aspects (2020), 125175.

[30] P. Meakin, Formation of fractal clusters and networks by irreversible diffusion-limited aggregation, Phys. Rev. Lett. 385 51 (13) (1983) 1119–1122.

[31] M. Lin, H. Lindsay, D. Weitz, R. Ball, R. Klein, P. Meakin, Letters to Nature, Universality in colloid aggregation, 1989.

[32] M. Lattuada, H. Wu, A. Hasmy, M. Morbidelli, Estimation of fractal dimension in colloidal gels, Langmuir 19 (15) (2003) 6312–6316.

[33] C.M. Sorensen, Light scattering by fractal aggregates: a review, Aerosol Sci. Technol. 35 (2) (2001) 648–687.

[34] J. Chaniot, M. Moreaud, L. Sorbier, T. Fournel, J. Becker, Tortuosimetric operator for complex porous media characterization, Image Anal. Stereol. (2019).

[35] L. Catita, E. Jolimaitre, A.-.A. Quoineaud, O. Delpoux, C. Pichon, J.-.M. Schweitzer, Mathematical modeling and magnetic resonance imaging experimental study of the impregnation step: a new tool to optimize the preparation of heterogeneous catalysis, Microporous and Mesoporous Mater. 312 (2021), 110756.

[36] G.A. Ledezma Lopez, J.J. Verstraete, L. Sorbier, A. Glowska, D. Leinekugel-Le-Cocq, E. Jolimaitre, C. Jallut, Generation of gamma-alumina digital twins using a nitrogen porosimetry simulation, Ind. Eng. Chem. Res. 60 (2021).

[37] D.R.E. Snoswell, J. Duan, D. Fornasiero, J. Ralston, Colloid stability and the influence of dissolved gas, The J. 400 Phys. Chem. B 107 (13) (2003) 2986–2994.